Adsorption Investigation of Boron Nitride Nanoparticle as Biodegradable Drug Delivery Carriers for the Mercaptopurine Anti-cancer Drug by Density Functional Theory

N. Masnabadi[1*], M. Samadizadeh[2], L. Sardarzadeh[2]

[1] Department of Chemistry, Roudehen Branch, Islamic Azad University, Roudehen, Islamic Republic of Iran
[2] Department of Chemistry, Central Tehran Branch, Islamic Azad University, Tehran, Islamic Republic of Iran

Abstract

Cancer is one of the most common diseases that affects many people around the world, and one of the challenges of the scientific community in dealing with cancer is to deliver drugs to cancerous tumors. Various reports show that boron nitride nanoparticles can be effective as drug nanocarriers and drug delivery in the target cell. In the present work, capsulation of anticancer drug of mercaptopurine (MCP) upon the boron nitride (6,6) nanotube, using DFT: B3LYP/6-31G* and the natural bond orbital analysis in the gas phase was investigated for the first time. Additionally, NCI analysis is used in this study to examine interactions between MCP and boron nitride nanotubes. To ascertain the impact of MCP adsorption into the nanotube, HOMO-LUMO orbitals, DOS (Density of States) plots, and molecular electrostatic potential maps (MEPs) were used. Furthermore, the effect of the abovementioned interactions between the drug and boron nitride nanotube on the electronic characteristics, and natural charges were estimated. Based on the gained results, the thermodynamic parameters of MCP nanotube and the results of NCI analysis were in close agreement with each other and it was also shown that the MCP adsorption process on the nanotube is a physical adsorption type, and the absorption process is associated with the release of heat, and it was in a favorable state in terms of thermodynamics. Furthermore, the results of IR spectra of drug, nanotube, and drug-nanotube mixture were investigated. Therefore, using boron nitride nanotube as a carrier for MCP drugs has been confirmed theoretically.

Keywords: Adsorption energy; Boron nitride nanotube; Density functional theory (DFT); IR spectra; Mercaptopurine.

Introduction

Nanotechnology as one of the most modern technologies in the world is used in some fields, such as materials engineering, medicine, drug design, biology, pharmacy, veterinary medicine, applied physics, semiconductors, super molecular chemistry, mechanical, electrical, chemical, and agricultural engineering (1-5).

* Corresponding Author: Tel: +989124493793; Email: Masnabadi@riau.ac.ir; NasMasnabadi@gmail.com

Researchers have begun to explore the use of nanotechnology in targeted medication delivery since its debut in pharmaceutical research. Nano–based drug delivery systems minimize the side effects of drug, and it is possible to achieve the proper loading of drug, and the favolable release features with low toxicity and long half-life and avoid wasting treatment time. Nanotechnology means the science of achieving the infrastructure of phenomena and the use of systems at the molecular level with new functions (5-8). Drug delivery is one of the most widely studied applications of nanotubes in biomedicine (8, 9). In recent years, different ways were developed to load small compounds such as anticancer drugs on nanotubes by covalent bonding or non-covalent adsorption.

Nanotubes-based nanomaterials are appropriate candidates for smart drug transport because they permit organized drug release in suitable sites. Encapsulation is a new technological method for packing solids, liquids, or gaseous substances in very small capsules floating in the water, their contents can be controlled in certain ways under certain conditions and the materials in the coating are protected from moisture, heat, or other conditions. The nanotubes can pierce the membrane and pass via it without damaging the cell membrane in terms of their sharp needle tip. The drug enclosed into the nanotube structure should be related to the size and diameter of the nanotube (10-12). Boron nitride nanotubes are biodegradable and non-toxic materials whose electronic properties do not depend on their chirality and diameter, and have high hydrophobicity, resistance to oxidation and heat, and were extensively researched in the applied fields of medicine and biomedicine (13-21).

Mercaptopurine (MCP) is an anticancer drug from the group of oral antineoplastic and antimetabolite drugs (22, 23). MCP is used in the treatment of acute myelomonocytic leukemia (AML), chronic myelocytic leukemia (CML), non-Hodgkin's lymphoma, polycythemia vera, inflammatory bowel and psoriatic arthritis diseases.

The metabolites of MCP and 6-thiovinosine monophosphate (T-IMP) are produced by the metabolism of MCP by hypoxanthine-guanine phosphoribosyl transferase (HGPRT) (24, 25).

This agent is incorporated into DNA as deoxythioguanosine, which leads to disruption of DNA replication. Besides, MCP is converted to ribonucleoside, 6-methyl mercaptopurine (MMPR) by 6-thiopurine methyltransferase (26). Using DFT simulations in the gas phase, Aslanzadeh (2018) examined the interaction of MCP with boron nitride nanotubes, nanosheets, and nanostructures. It was predicted that MCP tends to be physically absorbed in the surface of boron nitride

nanosheets with an absorption energy (E_{ad}) of about -3.2 kcal/mol. Boron nitride nanotubes have a shorter recovery time of about 49.5 seconds at room temperature, and this nanocarrier could be a good suggestion for use in MCP sensors (27).

Yang et al. showed the interaction of MCP with $B_{24}N_{24}$ nanoparticle using DFT calculations and presented an MCP nanosensor. They also found that the electrical conductivity of nanoparticle was significantly increased as a result of drug interaction with the nanoparticle (28).

This study prompted us to study the ability of B24N24 as an MCP drug carrier. To do this, we have investigated the interaction between MCP medication and boron nitride nanotube using density functional theory (DFT) simulations. The reactivity of MCP ($C_5H_4N_4S$) structure in the presence of boron nitride nanotube using quantum mechanical calculations (DFT) at B3LYP/6-31G* theoretical level was studied. Furthermore, how to place an arbitrary loading of MCP on the nanotube substrate with the lowest energy was studied. The physical adsorption of MCP in the presence of boron nitride nanotubes, and the electronic and mechanical properties of drug on the nanotube substrate were evaluated.

Materials and Methods

Increasing the efficiency and improving the properties of single boron nitride nanotubes (6, 6) ($B_{30}H_{24}N_{30}$), as nanocarriers for MCP ($C_5H_4N_4S$) is the main goal of this study. Gaussian 09 was used to obtain the optimum configuration of molecular structures, including MCP and boron nitride armchair nanotube (6,6) structures at B3LYP/6-31G* level of theories (29). Using the Gaussian software to scan the bonding angles and bonding distances between the drug and single-walled boron nitride nanotube, it was possible to detect the very stable electronic structure that resulted from the reaction of these compounds (30, 31). Thus, IR spectral results were studied with the B3LYP method and 6-31G* basis set. The analysis of molecular orbitals interaction, and state density diagrams for the mentioned compounds was performed by calculations at the theoretical level of B3LYP/6-31G* using NBO (Natural Bond Orbital) analysis (NBO 5.G software) (32, 33).

Results and Discussion
Optimization and Adsorption Energy
The structure of MCP ($C_5H_4N_4S$) and single armature boron nitride nanotubes (6,6) (B30H24N30) were optimized using standard B3LYP method with 6-31G * base set in the gas phase under standard conditions. The

structure of MCP was placed in different directions from the geometric structures of boron nitride nanotubes (6,6) with a length of 6 angstroms (single armature wall), and the electron energies of different mixtures of drugs with nanotubes were calculated by semi-experimental PM3 calculations. The optimal combination requiring the least amount of energy was discovered among all the investigated directions for the interaction between the MCP medication and boron nitride nanotube (Figure 1 and Table 1). Among all studied orientations for interaction, the most stable mixtures were Mix2 and Mix3.

Then, the stable electronic structure of MCP in Mix1 was optimized using theoretical calculations of DFT and using B3LYP method and 6-31G* basis set (Figure 2). The adsorption reaction between the drug and the
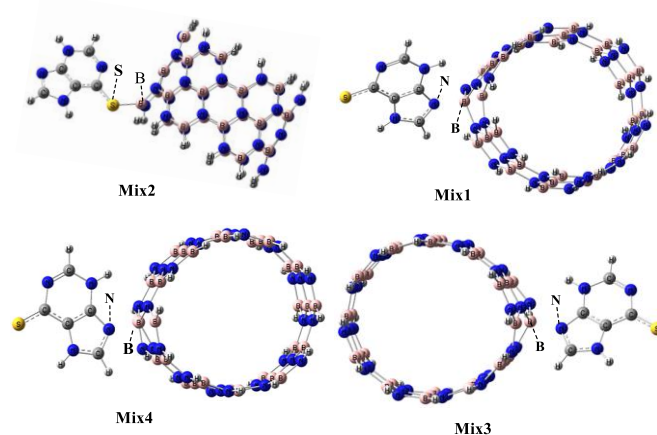

Figure 1. Structures resulted from the interaction of the MCP drug with boron nitride nanotubes

Table 1. Calculated energy values of MCP adsorption from different directions by boron nitride nanotube by PM3 method

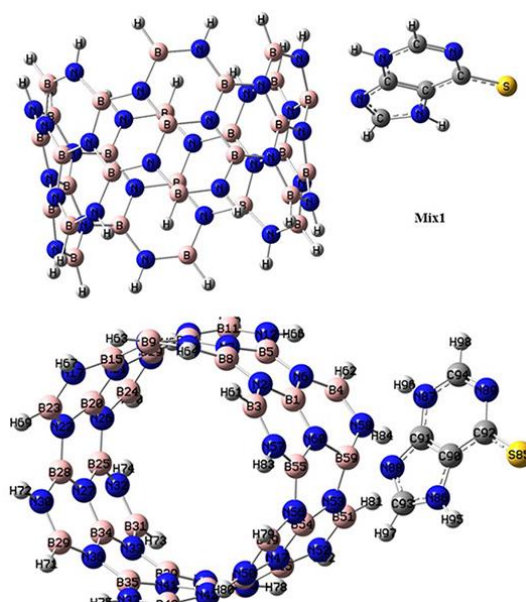| Mix MCP-nanotube	E_{el}
Mix1	-1492.002164
Mix2	-1491.564789
Mix3	-1491.564789
Mix4	-1491.28379

Figure 2. Structures resulted from the interaction of the MCP drug with boron nitride nanotubes with the lowest electron energy

nanotube is exothermic and can be performed in terms of energy (at the ambient temperature of 25°C and pressure of 1 atm) (Figure 2).

Based on Table 2, the optimized electron energy values of MCP drug, boron nitride nanotube (6,6), and MCP-boron nitride nanotube system (Mix1) wer-1e calculated -508368.394, -1509611.315 and -2017989.00 kcal.mol⁻¹, respectively. The values of thermodynamic parameters obtained in Table 2 show that when MCP drug is loaded on the boron nitride nanotube substrate, it becomes more stable than when considered in the absence of nanotubes. It means that loading the drug on boron nitride nanotubes makes the drug more stable. Therefore, based on Table 3, the adsorption energy (E_{ad}) of MCP by boron nitride nanotubes in the mixture (Mix1) in the gas phase is equal to 3.259 kcal.mol⁻¹. Therefore, it seems that MCP loading on boron nitride nanotube

substrate in the gas phase is exothermic and faceable (Figure 3).

The estimated thermodynamic parameters generally show that the MCP medication and boron nitride nanotube have a strong interaction. Based on the results obtained from the thermodynamic functions, the reaction related to the adsorption of MCP on the nanotube in the gas phase is exothermic, and the adsorption energy related to the drug-nanotube mixtures can be obtained from the following equations (1) to (4) (Table 3).

IR Spectroscopy

The IR spectra of drug, nanotubes, and Mix1 compounds were obtained using the results of vibration frequency calculations and are shown in Figures 4 to 6.

Table 2. Values of thermodynamic functions for MCP, boron nitride nanotube and MCP-boron nitride nanotube mixture in the gas phase in terms of kcal.mol⁻¹ and entropy in terms of cal.mol⁻¹K⁻¹ at B3LYP/6-31G* level of theory

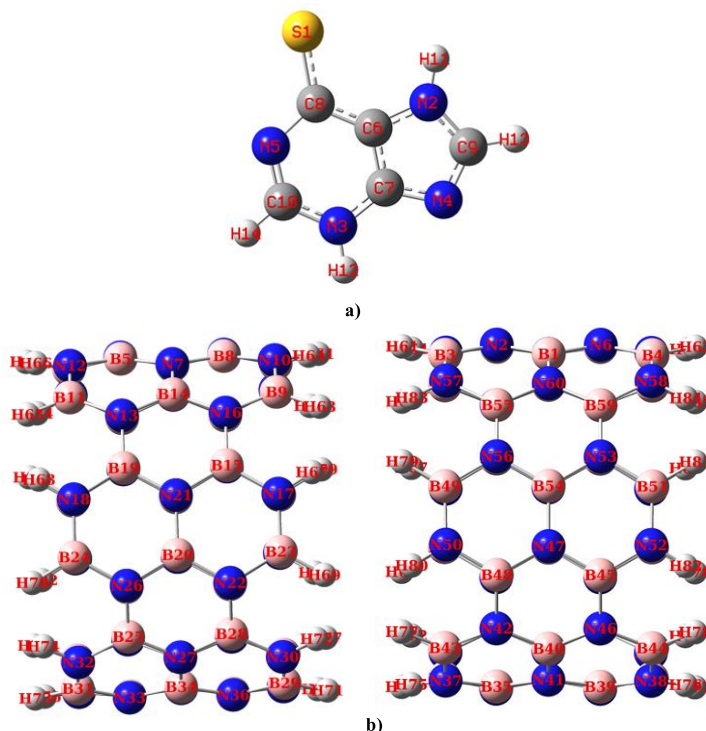| Compounds	$G+E_{el}$	$H+E_{el}$	$E_{Thermal}+E_{el}$	$E_0= ZPE+Eel$	E_{el}	S
MCP	-508327.228	-508301.790	-508302.382	-508306.884	-508368.394	85
nanotube	-1509284.055	-1509217.738	-1509218.330	-1509244.132	-1509611.315	222
Mix1	-2017608.024	-2017528	-2017528	-2017560.00	-2017989.00	269

a)

b)

Figure 3. Optimal structures; A) MCP b) Boron nitride nanotube (6,6-6) by computational method of B3LYP/6-31G*

Table 3 .Calculated adsorption energies of MCP on the surface of boron nitride nanotube in the gas phase at B3LYP/6-31G* level of theory

Thermodynamic Functions	ΔG	ΔH	ΔE_0	$\Delta E_{Thermal}$
	3.259	-8.472	-8.984	-7.636

Studying IR spectral results was performed by the Gaussian program (31), and in the IR spectrum of drug in the gas phase, the absorption band of the tensile vibration of C6 = C7 and C10 = N5 is observed in the area of $\upsilon = 1657$ cm^{-1}.

Symmetric and asymmetric vibrational frequencies of N-H have appeared in the regions of $\upsilon = 3618$ and $\upsilon = 3613$

cm^{-1}, respectively. The stretching vibration inside the plane of C = C and N-H bonds has appeared in $\upsilon = 1624$ cm^{-1}. The weak peaks in the areas of $\upsilon = 1405, 1202,$ and 1076 cm^{-1} are related to bending vibration of N-C, stretching vibration of C = S, and bending vibration inside the plane of N-C and N-H, respectively. The bands that appeared in $\upsilon = 561$ cm^{-1} and $\upsilon = 588$ cm^{-1}
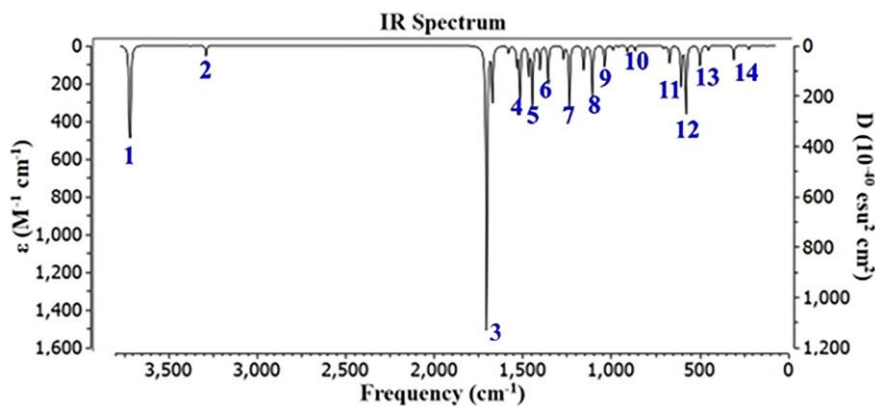

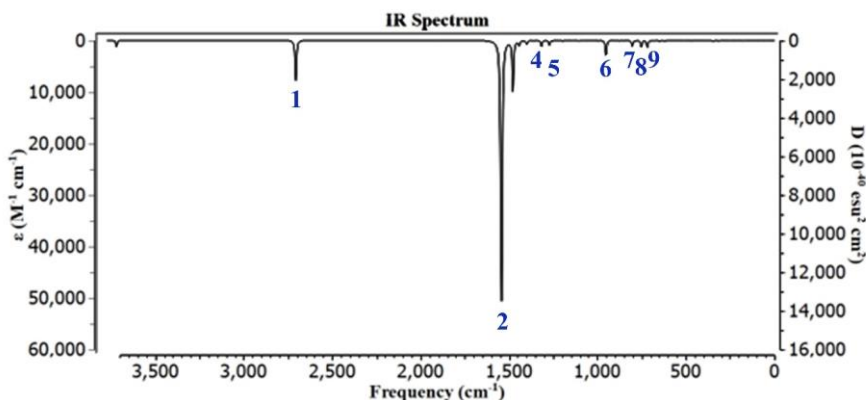**Figure 4**. IR spectrum of the MCP drug in the gas phase

Figure 5. IR spectrum of the Boron nitride nanotube (6,6-6) in the gas phase
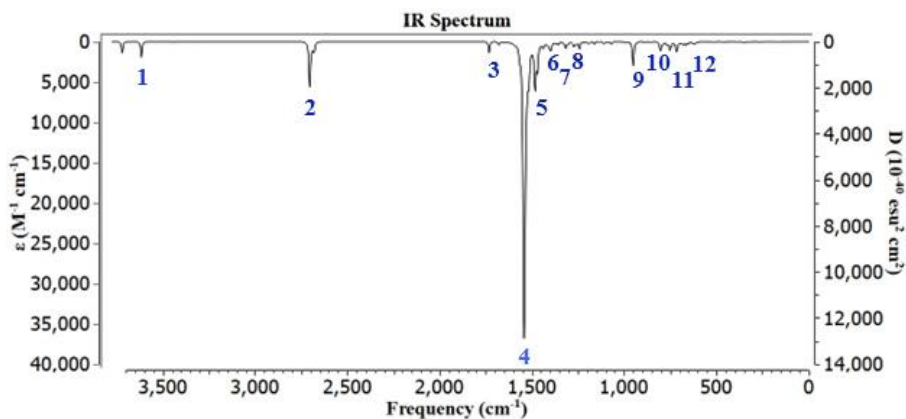

Figure 6. IR spectrum of MCP- Boron nitride nanotube mixture in the gas phase

29

corresponds to the bending vibration outside the plane of C-H and C = S bonds, respectively. Also, a weak peak in the region of $\upsilon = 931$ cm^{-1} is due to the stretching vibrations of C-H bonds. The appeared bands in $\upsilon = 3284$ cm^{-1} and $\upsilon = 3197$ cm^{-1} are due to the stretching vibrations of C-H (Figure 4).

The research has confirmed that the stretching peak for N-H in the imidazole and pyrimidine rings is placed on the regions 3522 and 3375 cm^{-1} in the IR spectrum for the MCP. The obtained our theoretical results showed imidazole and pyrimidine rings 3613 and 3618 cm^{-1}, respectively. According to the literature (34), the sharpest peak at 1619 cm^{-1} for C=N stretching is related to imidazole, and our results showed that this peak appeared at 1657 cm^{-1} and is the sharpest peak, too. Ring shifted to low frequency for all pyrimidine in terms of the deprotonation of the rings, increasing the shifting value illustrated to complete deprotonation. According to, an experimentally report (34), C=S stretching vibrations have appeared in 1192 cm^{-1} and our results show that this peak locates in 1234 cm^{-1}. Therefore, these theoretical results are in the same region as the experimental results and confirm each other.

Very weak peak in $\upsilon = 3606$ cm^{-1} is related to the stretching vibration of N-H bonds. The stretching vibration frequency of B = N and B-H bonds has appeared in the region of $\upsilon = 2627$ cm^{-1}. The sharp peaks that appeared in the region of $\upsilon = 1523$ cm-1 and $\upsilon=1521$ cm-1 are related to the stretching vibrations of B – N – B bonds. In the regions of $\upsilon = 1476$, 1416, and 1456 cm^{-1}, the bending vibrations of N-H bonds are observed. Thus, in the regions of $\upsilon = 778$ and 696 $\upsilon=696$ cm^{-1}, the bending vibrations of N-H bonds, and in the region of $\upsilon=965$ cm^{-1}, the bending vibrations of B-H bonds have appeared (Figure 5).

The IR spectrum of MCP-boron nitride nanotube mixture shows that the maximum vibration in the mix is related to bending vibration of N-H and the stretching vibration of B-N in the region of $\upsilon = 1436$ cm^{-1}. Additionally, a strong and sharp band corresponding to N-H bending vibration of the nanotube occurred in the 1493 cm-1 and 1498 cm-1 regions. This vibration altered in the presence and absence of MCP drug ($\omega = 1399$ cm-1) as a result of interactions between the drug and nanotube. The bending vibration of N-H and stretching vibration of B-N of nanotubes were observed in the band of 1493 cm^{-1}. The vibration of the double bond (for the MCP drug) in the mix structure appeared in the region of 1679 cm^{-1}, while this vibration appeared at the frequency (1624 cm^{-1}) in the absence of the nanotube. The increase in double bond frequency in the mixed structure was due to the decrease in the strength of MCP double bond as a result of the interaction with the tube. The C-H stretching

vibrations of MCP in the absence of a nanotube and its presence appeared in the bands of 3197, 3284 cm$^{-1,}$ and 3208, 3331 cm^{-1}, respectively. Increasing the stretching vibration frequency of the C-H in the structure of MCP in the presence of nanotubes is due to the reduction of C-H bond length. N-H absorption band of MCP in the absence and presence of boron-nitride nanotubes appeared in the regions of 3618 and 3607 cm^{-1}, respectively. The presence of nanotubes leads to a decrease in the frequencies of MCP N-H bonds, and in other words, the mentioned bond length increases.

It can be concluded that MCP was interacted with the nanotube. Moreover, C=S frequency did not change much in the absence and presence of nanotubes (Figure 6).

NBO Analysis and Stereo Electronic Effects

NBO analysis of electron wave functions are interpreted in terms of a series of occupied Lewis's orbitals and a set of unoccupied Lewis's orbitals (35). The new molecules' orbitals are more stable than pure Lewis's orbitals, which are associated with the stabilization of electron wave functions. Non-covalent electron deployment results in a consequence that is linked to the interaction between the orbitals of the electron donor and acceptor molecules. Therefore, it is natural to consider them as (donor-acceptor) charge transfer with the generalized Lewis-base Lewis acid type.

NBO analysis of interactions (bonding-anti-bonding) at the theoretical level of B3LYP/6-31G* shows that the highest resonant energy for MCP-nanotube boron nitride mixture is in terms of electron instability N86-C90 → BD*(2) and S85-C92→ BD*(2) (E39 = 393.18 kcal.mol^{-1}) that attributed to the electron transfer from MCP to boron nitride nanotubes (Table 4). The sum of resonance energy (stability) caused by electron destabilization from MCP drug to boron nitride nanotube (202.75 kcal.mol^{-1}) is more than electron destabilization from boron nitride nanotube to MCP drug (18.14 kcal.mol^{-1}), and the stability of the MCP-boron nitride nanotube mixture increases with the increase of electronic resonance (Figure 7 and Table 4).

The values of (Fi,j) obtained from NBO calculations for the electron displacement of BD*(2) N86-C90 → BD*(2)S85-C92 in MCP-boron nitride nanotube mixture was 0.097. For pure MCP drugs, the highest value of resonant energy is related to the electron transfers of BD(2)N4-C9→BD*(2)C6-C7 with E2 = 67.39 kcal.mol^{-}

Table 4. Resonance energies, energy difference of orbitals, and orbital overlap obtained at B3LYP/6-31G* level of theory (related to MCP in the absence and presence of boron nitride nanotube)

MCP				
Donor NBO (i)	**Acceptor NBO (j)**	**E(2)/ kcal/mol**	**ΔE/ a.u.**	**F(i,j)/a.u.**
BD (2) N 4 - C9	BD*(2) C 6 - C 7	24.98	0.33	0.087
BD (2) N 5 - C10	BD*(2) S 1 - C 8	24.15	0.28	0.080
BD (2) C 6 - C7	BD*(2) S 1 - C 8	28.26	0.24	0.076
BD (2) C6 - C7	BD*(2) N 4 - C 9	14.81	0.26	0.057
LP (2) S 1	BD*(1) N 5 - C 8	11.96	0.62	0.078
LP (1) N 2	BD*(2) N 4 - C 9	55.89	0.26	0.109
LP (1) N 2	BD*(2) C 6 - C 7	35.00	0.29	0.090
LP (1) N 3	BD*(2) N 5 - C10	49.68	0.29	0.111
LP (1) N 3	BD*(2) C 6 - C 7	40.99	0.3	0.100
LP (1) N 5	BD*(1) N 3 - C10	17.18	0.76	0.104
BD(2) N 4 - C9	BD*(2) C 6 - C 7	24.98	0.33	0.087
BD*(2) S 1 - C 8	BD*(2) N5 - C10	51.78	0.04	0.071
BD*(2) S1 - C8	BD*(2) C 6 - C 7	61.66	0.05	0.079
BD*(2) N4 - C 9	BD*(2) C6 - C7	67.39	0.03	0.062
MCP in Mix1				
Donor NBO (i)	**Acceptor NBO (j)**	**E(2)/ kcal/mol**	**ΔE/ a.u.**	**F(i,j)/a.u.**
BD (2) S 85 - C92	BD*(2) N86 -C 90	13.5	0.2	0.059
BD (2) N86 -C90	BD*(2) N87 -C91	13.47	0.3	0.068
BD (2) N86 - C90	BD*(2) N 88 - 93	33.88	0.32	0.099
BD*(2)N86 -C90	BD*(2) S 85 - C92	393.18	0.02	0.097
BD*(2) N86-C90	BD*(2) N 88 -C93	245.88	0.01	0.062
BD (2) N87 -C91	BD*(2) N 89 -C94	28.92	0.37	0.094
BD (2) N88 -C93	BD*(2) N87 - C91	30.14	0.29	0.101
BD (2) N89 - C94	BD*(2) S85 - C 92	24.75	0.28	0.08
LP (2) S 85	BD*(1) N89 - C92	12.13	0.62	0.078
LP (1) N 89	BD*(1) N87 - C94	17.17	0.77	0.104
BD*(2) S85 -C 92	BD*(2) N89 - C94	45.62	0.05	0.07
BD*(2) N 87 -C91	BD*(2) N88 - C93	319.26	0.01	0.071
BD*(2) N87 -C 91	BD*(2) N89 - C94	36.93	0.06	0.06
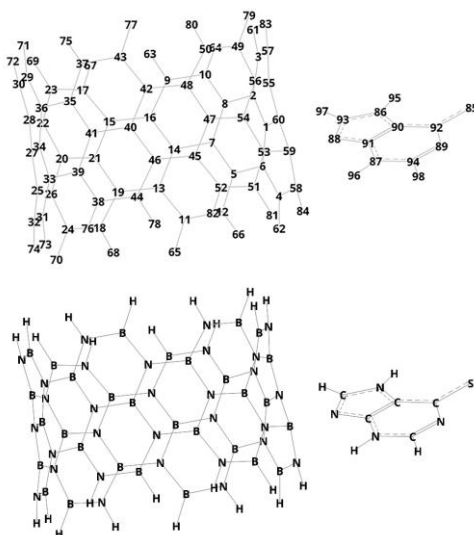
Figure 7. Numbering of atoms in the Mix1 structure

[1], BD(2)S1-C8→BD*(2) C6-C7 with E2 =66.61 kcal.mol^{-1} and Lp(1)N2→ BD*(2)N4-C9 with E2 = 67.67 kcal.mol^{-1} and the lowest value of resonant energy is related to electronic transfers of BD(1)N3-

Table 5. Resonance energies, energy difference of orbitals, and orbital overlap rate using DFT calculations at B3LYP/6-31G* level of theory (related to Mix1)

Donor NBO (i)	Acceptor NBO (j)	E(2) kcal.mol^{-1}	E(j)-E(i) a.u.	F(i,j) a.u.
From nanotube to MCP				
BD (1)N53-B59	BD*(1)N88 -C91	1.85	1.05	0.04
BD (1)N58 - B59	BD*(1) N88-C93	1.38	1.13	0.035
BD(2)N58 - B59	BD*(1)N87- H96	3.14	0.66	0.043
BD*(2) N58 - B59	BD*(1) N88-C91	1.72	0.3	0.046
BD*(2)N58 - B59	BD*(1)N88 -C93	3.49	0.33	0.069
From MCP to nanotube				
BD(1)N88 -C91	BD*(2) N58-B59	7.91	0.97	0.086
BD(1)N88 - C93	BD*(1)N53B59	1.49	1.26	0.039
BD (1)N88 - C93	BD*(2)N58 -B59	8.44	0.99	0.09
LP (1)N88	BD*(1)N53 -B59	21.22	0.87	0.131
LP (1) N 88	BD*(1)N58 -B59	4.32	0.89	0.06
LP (1) N 88	BD*(2) N58-B59	149.6	0.61	0.27

C10→BD*(1)N5-C10 and BD(1)N3-H12 →BD* (1) N3-C7 with E2 = 0.52 kcal.mol^{-1}. For MCP in the Mixed structure with boron nitride nanotubes, the highest value of resonant energy is related to the electron transfers of BD* (2) N86-C90 → BD* (2) S 85 -C 92 with E2 = 393.18 kcal.mol^{-1}, BD * (2) N86-C90 BD* (2) N88 -C 93 with E2 = 258.88 kcal.mol^{-1} and BD (2) N88-C93 → BD * (2) N87-C91 with E2 =30.14 kcal.mol^{-1} and BD (2) N87-C91 → BD * (2) N89-C94 with E2 =28.92 kcal.mol^{-1} (Table 4).

Table 5 presents the parameters derived from the NBO analysis, which consist of resonant energies associated with electron transfer, energy difference between orbitals, and the extent of orbital overlap between the drug and the nanotube, as well as from the nanotube to the drug. Thus, based on the obtained values, the electron transfers from drug to nanotube are more than the electron transfers from nanotube to drug, and the highest electron transfer from drug to nanotube is related to electron transfer of LP(1)N88→BD*(2)N58-B59, which has an energy equivalent of 149.6 kcal.mol^{-1}.

Structural Parameters

Structural parameters calculated using the computational method of B3LYP/6-31G* for pure MCP and drug in the presence of boron nitride nanotubes (Mix1) are observed in Tables 6 and 7. A comparison of calculated structural parameter changes of MCP in the presence and absence of nanotubes reveals that the interaction-involved regions experience a significant change in structure. Based on the obtained results of calculations, there is a direct relationship among the changes in structural parameters and the resonant energy values due to the electron displacement. The higher the resonance energy due to electron transfers in a bond, the greater the change in the structural parameters of that bond. Thus, when MCP reacts with the surface of boron nitride nanotubes, the highest resonant energy is due to the electron displacement of LP (1) N88 → BD * (2) N58-B59 (E14= 149.63 kcal/mol) and LP (1)N88→BD*(1)N53-B59 (E2 = 21.22 kcal/mol) which is related to the electron transfers from the drug to boron nitride nanotubes (Tables 5). In the MCP-boron nitride nanotube mixture, bond length of $r_{C93-N86}$ =1.347 has become shorter than the same bond in the drug r_{C9-N2} =1.361) and the bonds length of r_{C9-N2} =1.336, $r_{C90-C91}$ =1.379, $r_{N87-H96}$ =1.019 and $r_{C91-N88}$ =1.368 are shorter for the same bonds in the drug (r_{C9-N4} =1.329 and r_{C6-C7} =1.387, r_{N3H12} =1.012 and r_{C7-N4} =1.359). Thus, in MCP-boron nitride nanotube mixture, the bond length of $r_{C91-N87}$ = 1.363 has become larger than the same bonds in boron nitride nanotubes (rC7-N3 = 1.372).

In MCP-boron nitride nanotubes, bond angles of θN87-C91-C90=119.7, θC91C91-N88-C93=105.2, θC90-N86-C93=108.3, θH97-C93-N86=125.0 and θH96-N87-C94=125.1, has become shorter than these bond angles angle in the drug (θN3-C7-C6=118.2 and θC7-N4-C9=103.1, θC6- N2-C9=107.1, θH13-C9-N2=122.4, θ H12-N3-C10=122.). Also, the bond angles of θN88-C93-N86=111.1, θH95-N86-C93=128.2 and θH96-N87-C9=118.5, respectively, has become larger than these angles in MCP (θN4-C9-N2=113.1 and θH11-N2-C9=129.2 and θH12-N3-C7=121.1).

In MCP-boron nitride nanotube mixture, the dihedral angles of φH96-N87-C94-H98=5.7 and φH9-N87-C91-N88=4.9 in the mixture have become shorter than these angles in MCP (φH12-N3-C10-H14=0.0 and φH12-N3-C7-N4=0.0).

Moreover, the electron transfers of resonant energy related to the electron transfers of BD*(2) N86-C90 → BD * (2) S85-C92 with E2 =183.393 kcal.mol^{-1}, BD*(2)

Table 6. Optimized values of bond length of MCP in the absence and presence of boron nitride nanotubes (in Mix1) at B3LYP/6-31G* level of theory

MCP		MCP in Mix1		ΔBond lengths (MCP- MCP in Mix1)
Bonds	**Bond lengths (Å)**	**Bond**	**Bond lengths (Å)**	
C6-C7	1.387	C90-C91	1.379	0.008
C7-N4	1.359	C91-N88	1.368	0.009
C7-N3	1.372	C91-N87	1.363	0.009
C9-N2	1.361	C93-N86	1.347	0.014

Table 7. Optimized values of bond angles of MCP in the absence and presence of boron nitride nanotubes (in Mix1) at B3LYP/6-31G* level of theory

| MCP		MCP in Mix1		ΔBond lengths (MCP- MCP in Mix1)
Angle	**Bond angle (°)**	**Angle**	**Bond angle (°)**	
N3-C7-C6	118.192	N87-C91-C90	119.727	1.53
C7-N4-C9	103.113	C91-N88-C93	105.251	2.13
N4-C9-N2	113.127	N88-C93-N86	111.105	2.02
C6-N2-C9	107.105	C90-N86-C93	108.275	1.17
H13-C9-N2	122.369	H97-C93-N86	125.044	2.67
H11-N2-C9	129.190	H95-N86-C93	128.186	1.004
H12-N3-C10	122.001	H96-N87-C94	125.089	3.08
H12-N3-C7	121.071	H96-N87-C91	118.503	2.56

N86- C90 → BD * (2) N88 -C93 with E2 = 245.88 kcal.mol^{-1}, BD*(2)N86-C90 → BD*(2) N88 -C93 with E2 =245.88 kcal/mol and BD(2) N88 - C93 → BD*(2) N87-C91 with E= 30.14 kcal.mol^{-1} is for MCP drug in the presence of the boron nitride nanotubes that cause to changes in the bonds length, the bond angles and the dihedral angles.

Therefore, one approach to explain physical absorption by electron displacement between the two systems participating in this interaction might be through modifications to structural characteristics.

Molecular Electrostatic Potential
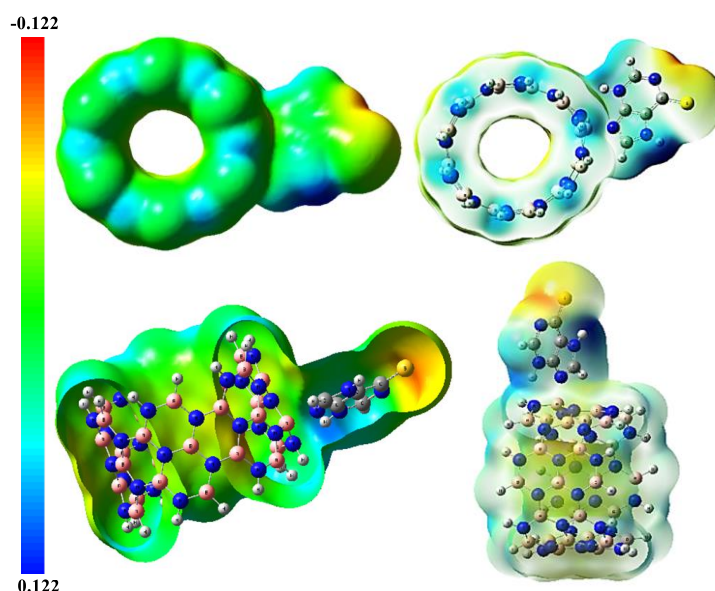
Figure 8. Scheme of molecular electrostatic potential map (MEP) calculated by B3LYP/6-31G* for MCP-boron nitride nanotube in Mix1 (in base state)
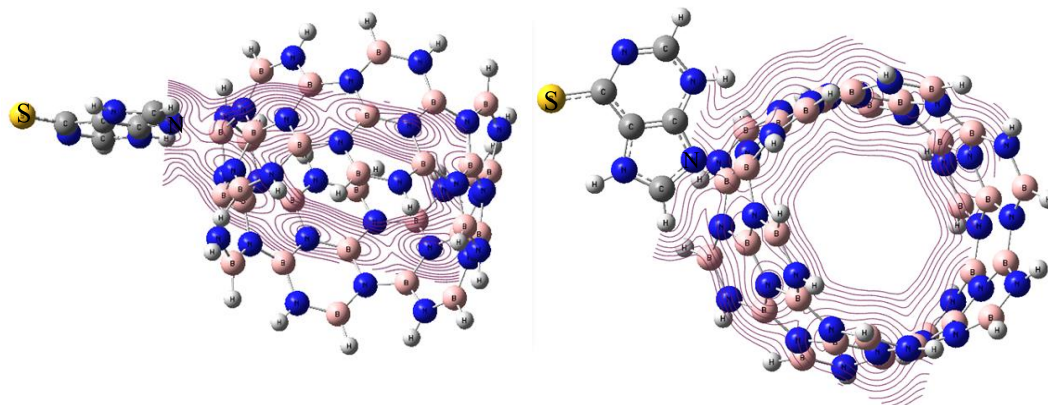
Figure 9. Transfers lines indicating contours showing the range of atoms.

One of the useful strategies for studying reactivity is plotting a molecular electrostatic potential map (MEP). A MEP is used to show the size of the molecule, the shape of the molecule as centers with negative and positive electrostatic potential, and a range of color changes (36). In general, the nucleophilic and electrophilic regions in a structure are characterized by electrostatic potential, and it is possible to predict the active regions in the reaction. In Mix1, a positive charge density is dominant on the atoms of MCP drug, which conduct the charge density to the reaction center (sulfur atoms and nitrogen atoms on the MCP drug) by electron resonance, and themselves are far from the reaction center. The negative charge density is predominant on the sulfur atom and the N86 atom on the MCP involved in the reaction. Therefore, reactive centers are identified in this complex (Figures 8 and 9).

LUMO and HOMO orbitals (FMO) have a important role in charge transfer process in molecules and the chemical reactions. The HOMO and LUMO energies display the ability of the orbital to donate and obtain an electron, respectively. The energy gap between HOMO and LUMO orbitals is a major factor in the designation of the electrical transport properties in molecules (37). Considering the results of FMO analysis, the energy gap between LUMO and HOMO orbitals of the pure drug is 3.695eV, while after the capsulation with the nanotube, it decreased up to about 3.631 eV (Figures 9 and 10).

The quantum molecular descriptors, including electron affinity (A), ionization potential (I), electronegativity (χ), electrophilicity (ω), global hardness (η), electronic chemical potential (μ), and chemical softness (S) are calculated according to following equations, for the studied compounds (38)):

$$[I = -E_{HOMO}], \ [A = -E_{LUMO}],$$
$$[\eta = I - A/2], \ [\chi = (I+A)/2],$$
$$[\mu = -(I+A)/2], \ [\omega = \mu^2/2\eta], \ [S = 1/2\eta] \quad (1)$$

Hardness is a factor that states chemical reactivity and determines molecules' stability. The global hardness values (η) for the drug are reported as 1.84 eV, in Table 8. With capsulation of the MCP drug on nanotube, the
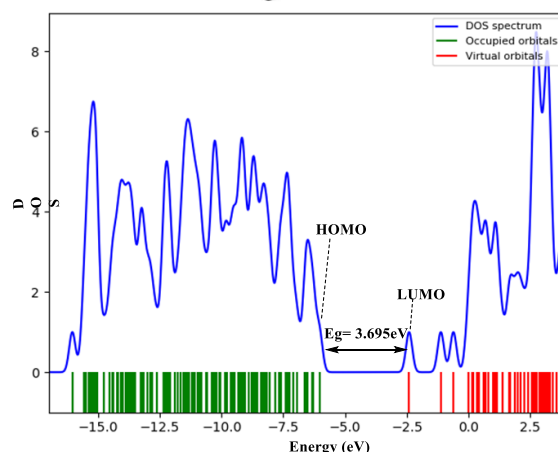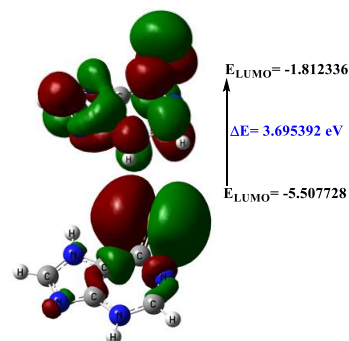

Figure 10. DOS diagram of MCP - boron nitride nanotube (Mix2)

34

Table 8 .Optimized values of bond angles of MCP in the absence and presence of boron nitride nanotubes (in Mix1) at B3LYP/6-31G* level of theory

MCP		MCP in Mix1		△Bond lengths
Angle	Bond angle (°)	Angle	Bond angle (°)	(MCP- MCP in Mix1)
N3-C7-C6	118.192	N87-C91-C90	119.727	1.53
C7-N4-C9	103.113	C91-N88-C93	105.251	2.13
N4-C9-N2	113.127	N88-C93-N86	111.105	2.02
C6-N2-C9	107.105	C90-N86-C93	108.275	1.17
H13-C9-N2	122.369	H97-C93-N86	125.044	2.67
H11-N2-C9	129.190	H95-N86-C93	128.186	1.004
H12-N3-C10	122.001	H96-N87-C94	125.089	3.08
H12-N3-C7	121.071	H96-N87-C91	118.503	2.56

global hardness value in the CMP-nanotube complex improved (1.81 eV). The capsulated drug becomes more reactive and its kinetic stability decreases until it reaches the patient's tissue. Therefore, the electrophilicity (ω) of the CMP-nanotube complex decreased than that of the pure drug. Therefore, the energy gap value for MCP drug is reduced with capsulation from 3.69 eV to 3.63 eV. The quantity (ΔN) shows the amount of charge transfer in the MCP-nanotube complex, which according to its positive values (ΔN>0), indicates the transfer of electrons from the boron nitride nanotube (as an electron donor) to MCP drug (as an electron acceptor). Therefore, this fact is a confirmation that the LUMO orbital distribution is on the drug and the HOMO orbital distribution is on the nanotube.

Also, the energy gap has a significant effect on the reactivity of the molecule (39, 40). Stability and stabilization of orbital interactions may be associated with increasing and decreasing the energy levels of the electron-donor and electron-acceptor orbitals, respectively. The population of electron donor and acceptor orbitals is changed by electron instability, which is a confirmation of electron instability. Figures 10 and 11 show the energy gap of the HOMO-LUMO molecular orbitals, as well as the DOS diagram. Examination of the molecular orbitals of the MCP drug shows that HOMO orbital is on the C = S group and the LUMO orbital is spread over the entire structure of MCP molecule. It is predicted that the possibility of reacting with electrophilic species is in the part where the distribution of HOMO orbitals is more and the possibility of reacting with nucleophilic species is in the part where LUMO orbitals are more distributed (41). The HOMO orbitals are more broadly dispersed on the nitrogen atoms while the LUMO orbitals are situated on the boron atoms, according to the molecular orbital form of boron nitride nanotubes. When the drug is placed on the nanotube, its HOMO and LUMO distribution orbitals change compared to the mixture of drug and the nanotube, and this indicates a change in the reactivity behavior of the

drug. That is, the reactive centers have been changed by placing them on the nanotube. The concentration of LUMO orbitals in the above positions indicates that these points are suitable for the attack of nucleophiles.

In this work, non-covalent interaction index (NCI) studies were used to detect the type and measure the amount of intermolecular interactions between MCP drug molecules and borderron nitride nanotubes of the drug delivery system. Checking this index is done through calculations with the following equation (42):

$$RDG(r) = \frac{1}{2(3\pi^2)^{1/3}} \frac{|\nabla\rho(r)|}{\rho(r)^{4/3}}$$

(2)

The dispersion value of the reduced electron density

E_{LUMO}= -2.40584 eV

ΔE= 3.631eV

E_{HOMO}= -6.036768 eV
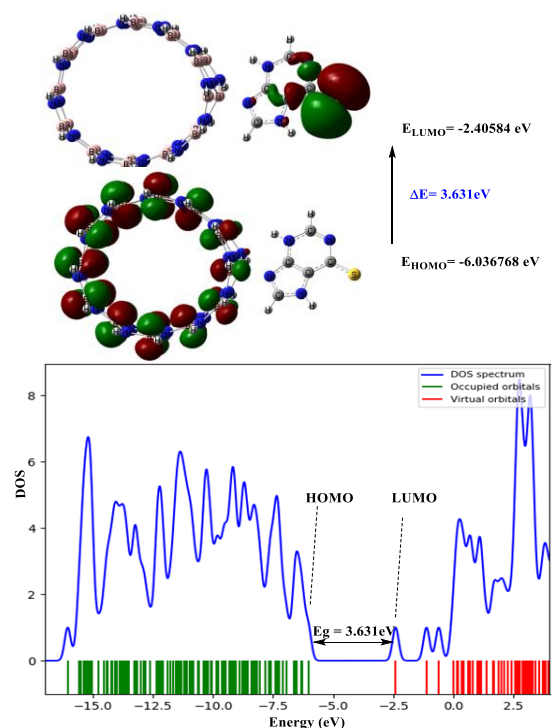
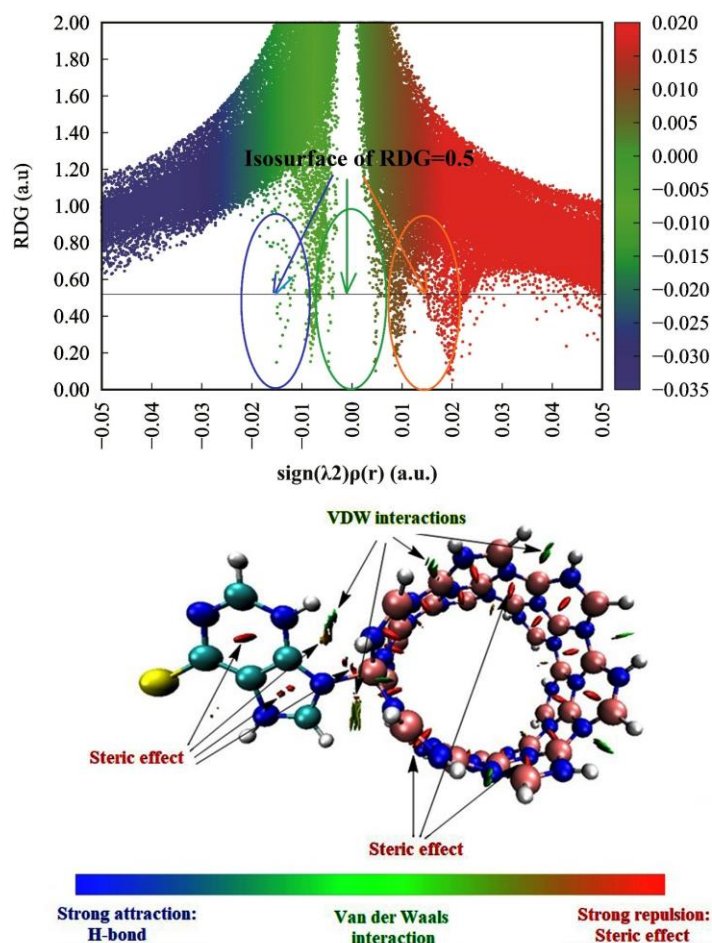**Figure 11**. DOS diagram of MCP-boron nitride nanotube (Mix3)

Figure 12. Reduced electron density gradient (RDG) isosurface map of the MCP-boron nitride nanotube complex. The values of Sign ($\lambda 2$) in the surfaces are represented by variation of color according to the color bar.

gradient (RDG) on the Y axis is plotted as a unit graph against the electron density parameter (ρ) multiplied by the sign ($\lambda 2$) on the X axis and is shown in Figure 4. Multiwfn program (43) was used to determine the sign ($\lambda 2$)ρ(r) and NCI–RDG. To separate the non-bonded interactions ($\lambda 2 > 0$) from the bonded type ($\lambda 2 < 0$), the sign ($\lambda 2$)ρ(r) is used. It should also be determined that non-covalent interactions will result in low RDG values (44). The RDG parameter is a measure to detect the deviation from the uniform distribution of electrons and is obtained from the first derivative of the electron density. The green areas indicate the presence of places with weak electron density and weak intermolecular interactions in the RDG scattering diagram. Spatial interactions are marked in red in the diagram. The density gradient at critical points with weak interactions vanishes and peaks are seen in the NCI plot. Therefore, RDG scattered dots in blue color were used to display H-bonding interactions in the negative

dominion (43, 44). The NCI diagram of the formed drug delivery system (Figure 12) confirms the weak interaction between the MCP drug and the boron nitride nanotube. However, there are areas of green ISO surface in the NCI chart. The steric effect interactions between aromatic rings on the drug and boron nitride nanotubes are associated with another regional redn. In addition, there is a distinct combination of red and green colors in the RDG design. Therefore, obtaining weak intermolecular interactions (van der Waals interactions) between the drug molecules and the BNNT nanocarrier is the result of this study. The presence of green areas inside the nanocarrier containing MCP indicates the interactions between these two components of the drug delivery system. It should also be checked that MCP drug compounds and boron nitride nanocarriers have aromatic structures that have a significant effect on creating van der Waals interactions, as can be understood from the

strong RDG spikes in Figure 12.

Conclusion

In this study, the interaction between MCP and boron nitride nanotubes was studied theoretically. The results of initial method (DFT) calculations were performed at B3LYP/6-31G* theoretical level and NBO analysis. The study's findings include the reactivity of MCP in the presence of boron nitride nanotubes as well as structural, bonding, energetic, and stereoelectronic interactions. The stable electronic structure of the mixture of MCP and boron nitride nanotubes was determined by scanning the bonding angles, and the bond distance between MCP and boron nitride single-walled nanotubes using calculations at B3LYP/6-31G* theoretical level. Based on the gained results from calculations of B3LYP/6-31G* theoretical levels, the parameters of enthalpy (ΔH) and Gibbs free energy (ΔG) changes were calculated, which partly explained the endothermic nature of the reaction. The improvement in stability of the MCP-boron nitride nanotube combination is also successfully determined by electron stereo effects, which are induced by electron instability. By comparing the numerical value of Fi,j (resonance energy value) obtained for electron transfers, it can be concluded that the increase in orbital overlap justifies the increase in resonance energy in terms of electron instability. There is a direct relationship between the changes in geometric parameters and resonant energies due to the calculated electron displacement, so changes in structural parameters can be one way to justify the physical adsorption reaction through electronic transitions between two systems involved in the reaction.

The consequences of B3LYP/6-31G* computation show that in examining the shape of the molecular orbitals of the MCP drug, it is observed that the HOMO orbital is on C=S group and the LUMO orbital is extended over the entire structure of the MCP molecule. It is predicted that the likelihood of reacting with electrophilic species is greater in the region where LUMO orbitals are more dispersed and disseminated, while the likelihood of reacting with nucleophilic species is greater in the region where HOMO orbitals are more widely distributed. The shape of the molecular orbitals of boron nitride nanotubes shows that LUMO orbitals are located on the boron atoms and the HOMO orbitals are more widely distributed on the nitrogen atoms.

Also, studying the electrostatic potential map in MCP-boron nitride nanotube mixture showed that the positive charge density is dominant on the atoms of the MCP drug which conduct the charge density to the reaction center (sulfur atoms and nitrogen atoms on the MCP drug) by electron resonance and are far from the reaction center, and the negative charge density on the

sulfur atom and 86 nitrogen atoms of the MCP involved in the reaction is dominant, and thus the reactive centers in this complex are determined. Loading of MCP on the boron nitride nanotube surface makes the drug to be more stable on the nanotube. Based on the results, the adsorption energy of MCP on the boron nitride nanotubes (E_{ad}) was obtained equal to 8.259 kcal.mol^{-1} which shows that the reaction is endothermic. The system of MCP-boron nitride nanotube mixture with low adsorption energy is thermodynamically favorable and indicates the strong interaction of the drug with the boron nitride nanotube and the high stability of MCP-boron nitride nanotube mixture. By examining the energy gaps in the MCP and Mix1 mixture, it is observed that the semiconductor property of MCP increases to 0.06 electron volts as a result of interaction with boron nitride nanotubes, and this can have a suitable effect for optimal applications of encapsulation of the MCP drug and improve its chemical behavior.

References

1. Afzal O, Altamimi ASA, Nadeem MS, Alzarea S, Almalki WH, Tariq A, Mubeen B, Murtaza BN, Iftikhar S, Riaz N, Kazmi I, Nanoparticles in Drug Delivery: From History to Therapeutic Applications. Nanomaterials (Basel). 2022;12(24):4494.
2. Hong S, Choi DW, Kim HN, Park CG, Lee W, Park HH, Protein-Based Nanoparticles as Drug Delivery Systems. Pharmaceutics. 2020;12(7):604.
3. kianfar E. Magnetic Nanoparticles in Targeted Drug Delivery: a Review. Journal of Superconductivity and Novel Magnetism. 2021;34:1709-1735.
4. Stanicki D, Vangijzegem T, Ternad I, Laurent S. An update on the applications and characteristics of magnetic iron oxide nanoparticles for drug delivery. Expert Opinion on Drug Delivery. 2022;19(1):321-335.
5. Benita S. Microencapsulation Methods and Industrial Applications, 2nd Edition, USA: CRC Press, 2006.
6. Alromi DA, Madani SY, Seifalian A, Emerging Application of Magnetic Nanoparticles for Diagnosis and Treatment of Cancer. Polymers (Basel). 2021;13(23):4146.
7. Saugandhika M, Nathalia P."Impedance electrodes for Biological applications using carbon nanotubes [Thesis], George Mason University, 2007.
8. Weng CC, Yang TA, Li. YK. Design and fabrication of cell-targeted, dual drug-loaded nanoparticles with pH-controlled drug release and near-infrared light-induced photothermal effects. Materials and Design. 2021;197:109230.
9. Labhasetwar V, Song C and Levy RJ. Nanoparticle drug delivery system for restenosis. Advanced Drug Delivery Reviews. 1997;24:63-85.
10. Hossein Zare H, Ahmadi S, Ghasemi A, Ghanbari M, Rabiee N, Bagherzadeh M, Karimi M, Webster TJ, Hamblin MR, Mostafavi E. Carbon Nanotubes: Smart Drug/Gene Delivery Carriers. International Journal of Nanomedicine. 2021;16:1681–1706.

11. Rasul MDG, Kiziltas A, Arfaei B, Shahbazian-Yassar R. 2D boron nitride nanosheets for polymer composite materials. npj 2D Materials and Applications. 2021;56.

12. Li X, Hao X, Zhao M, Wu Y, Yang J, Tian Y and Qian G. Exfoliation of Hexagonal Boron Nitride by Molten Hydroxides. Advanced Materials. 2013;25:220-2204.

13. 13.Ciofani G, Danti S, Alessandro DD, Moscato S and Menciassi A. Assessing cytotoxicity of boron nitride nanotubes: Interference with the MTT assay. Biochemical and Biophysical Research Communications. 2010;394:405-411.

15. Li X, Zhi C, Hanagata N, Yamaguchi M, Bando Y and Golberg D. Boron nitride nanotubes functionalized with mesoporous silica for intracellular delivery of chemotherapy drugs. Chemical Communications. 2013;49:7337-7339.

14. Gupta A, Kumar S and Kashyap A. International Journal of Innovative Research in Science. Engineering and Technology. 2013;2:1209-1215.

15. Sletten E, Sletten J and Jensen LH. The Crystal and Molecular Structure of 6-Mereaptopurine Monohydrate. Acta Crystallography B. B 1969;25:1330-1338.

16. Sharifi KA and Pirsa S. Biodegradable film of black mulberry pulp pectin/chlorophyll of black mulberry leaf encapsulated with carboxymethylcellulose/silica nanoparticles: Investigation of physicochemical and antimicrobial properties. Materials Chemistry and Physics 2021;267:124580.

17. Sani IK, Geshlaghi SP, Pirsa S and Asdagh A. Composite film based on potato starch/apple peel pectin/ZrO2 nanoparticles/microencapsulated Zat -aria multiflora essential oil; investigation of physicochemical properties and use in quail meat packaging Food Hydrocolloids. 2021;117:106719.

18. Pirsa S. Biodegradable film based on pectin/Nano-clay/methylene blue: Structural and physical properties and sensing ability for measurement of vitamin C. International Journal of Biological Macromolecules. 2020;163:666-675.

19. Jabraili A, Pirsa S, Pirouzifard M and Amiri S. Biodegradable nanocomposite film based on gluten/silica/calcium chloride: physicochemical properties and bioactive compounds extraction capacity. Journal of Polymers and the Environment. 2021;25:1-5.

20. Hosseini SN, Pirsa S and Farzi J. Biodegradable nano composite film based on modified starch-albumin/MgO; antibacterial, antioxidant and structural properties. Polymer Testing. 2021;97:107182.

21. Pourmadadi M, Rahmani Ghohrodi A, Savari Z, Talebi E, Ahamdi I, Rahdar A, Pandey S. Enhancing cancer therapy: The potential of mercaptopurine-based nanomaterials for targeted drug delivery. Next Nanotechnology. 2023;2:100018.

22. Huyen DT, Bui TQ, Si NT, VuNhat P, Quy PT, Nhung NTA. Theoretical study of the binding mechanism between anticancerous drug mercaptopurine and gold nanoparticles using a cluster model. Journal of Molecular Modeling. 2023;29.

23. Shannon E. Conneely, Stacy L. Cooper, and Rachel E. Rau. Use of Allopurinol to Mitigate 6-Mercaptopurine Associated Gastrointestinal Toxicity in Acute Lymphoblastic Leukemia. Front Oncol. 2020;10:1129.

24. Wojtuszkiewicz A, Barcelos A, Dubbelman B, Abreu RD, Brouwer C, Bökkerink JP,de Haas V, Groot-Kruseman HD, Jansen G, Kaspers GL, Cloos J, Peters GJ. Assessment of Mercaptopurine (6MP) Metabolites and 6MP Metabolic Key-Enzymes in Childhood Acute Lymphoblastic Leukemia. Nucleosides, Nucleotides and Nucleic Acids. 2014;33:4-6.

25. Baskan EB, Yilmaz M, Tunali S and Saricaoglu H. Efficacy and safety of long-term mycophenolate sodium therapy in pemphigus vulgaris. Journal of the European Academy of Dermatology and Venereology. 2009;23:1432-1434.

26. Aslanzadeh SA. Adsorption of MCP drug on the BN nanotube, nanosheet and nanocluster: a density functional theory study. Molecular Physics. 2018;117:531-538.

27. Yang Y and Ostadhosseini N. A theoretical investigation on the MCP drug interaction with boron nitride nanocage: Solvent and density functional effect. Physica E: Low-dimensional Systems and Nanostructures. 2021;125:14337.

28. Frisch MJ, Trucks G, Schlegel HB, Scuseria GE, Robb MA and Cheeseman J. Antioxidant potential of glutathione: a theoretical study. Russian Journal of Physical Chemistry B. 2011;115:11269-11277.

29. Li Z, Wan H, Shi Y and Ouyang P. Personal Experience with Four Kinds of Chemical Structure Drawing Software: Review on ChemDraw, ChemWindow, ISIS/Draw, and Chem Sketch Journal of Chemical Information and Modeling. 2004;44:1886-1890.

30. Dennington R, Keith T and Millam J. Gauss View, Version 5. Semichem Inc., Shawnee Mission (2009).

31. Glendening D, Badenhoop JK, Reed AE, Carpenter JE, Bohmann JA, Morales CM, Weinhold F. Theoretical Chemistry Institute, University of Wisconsin, Madison WI, NBO version 5.G (2004).

32. Seminario JM and Politzer P. Eds., Modern Density Function Theory, a Tool for Chemistry, Elsevier, Amsterdam (1995).

33. Sharfalddin AA, Emwas AH, Jaremko M, Hussien MA. Transition metal complexes of 6-mercaptopurine: Characterization, Theoretical calculation, DNA-Binding, molecular docking, and anticancer activity. Applied Organometalic Chemistry. 2020;e6041.

34. Passos Gomes GD, Alabugin I, Stereoelectronic Effects: Analysis by Computational and Theoretical Methods. Applied Theoretical Organic Chemistry. 2018:451-502.

35. Suresh CH, Remya GS,| Anjalikrishna PK. Molecular electrostatic potential analysis: A powerful toolto interpret and predict chemical reactivity. WIREs Computational Molecular Science. 2022;12:e1601.

36. Hosseinzadeh M, Masoudi S, Masnabadi N, Azarakhshi F. Theoretical study of encapsulation of diethylstilbestrol drug into the inner surface of BNNT toward designing a new nanocarrier for drug delivery systems. Materials Research Express. 2022;9:045002.

37. Stern N, Major DT, Gottlieb HE, Weizman D, Fischer B. What is the conformation of physiologically-active dinucleoside polyphosphates in solution? Conformational analysis of free dinucleoside polyphosphates by NMR and molecular dynamics simulationsOrganic and Biomolecular Chemistry. 2010;8:4637–4652.

38. Masnabadi N. DFT study and NBO analysis of conformation properties of 2,5,5-trimethyl-1,3,2-

dioxaphosphinane 2-selenide and their dithia and diselena analogous. Journal of Sciences, Islamic Republic of Iran 2020;31:137-46.

39. Danaie E, Masoudi S, Masnabadi N A Computational Study of the Conformational Behavior of 2, 5-Dimethyl-1, 4-dithiane-2, 5-diol and Analogous S and Se: DFT and NBO Study. Letters in Organic Chemistry. 2020;1:749-59.

40. Parthasarathi R, Padmanabhan J, Elango M, Subramanian V. and hattaraj P.K. Intermolecular reactivity through the generalized philicity concept. Chemical Physics Letters. 2004;394:225-230.

41. Boto RA, Peccati F, Laplaza R, Quan C. NCIPLOT4: Fast, Robust, and Quantitative Analysis of Noncovalent Interactions. Journal of Chemical Theory and Computation. 2020;16(7):4150–4158.

42. Akman F, Demirpolat A, Kazachenko AS, Kazachenko AS, Issaoui N, Al-Dossary O, Molecular Structure, Electronic Properties, Reactivity (ELF, LOL, and Fukui), and NCI-RDG Studies of the Binary Mixture of Water and Essential Oil of Phlomis bruguieri. Molecules. 2023;28(6): 2684.

43. Saleh G, Gatti C, Presti LL. Non-covalent interaction via the reduced density gradient: Independent atom model vs experimental multipolar electron densities. Computational and Theoretical Chemistry. 2012; 998:148-163.

44. Johnson ER, Keinan S, Mori-Sánchez P, Contreras-García J, Cohen AJ, Yang W. Revealing noncovalent interactions. Journal of the American Chemical Society. 2010;132(18):6498-506.